

# Exploring the propagation of relativistic quantum wavepackets in the trajectory-based formulation

Hung-Ming Tsai and Bill Poirier

Department of Chemistry and Biochemistry, and Department of Physics,  
Texas Tech University, Box 41061, Lubbock, Texas 79409-1061, USA

E-mail: Bill.Poirier@ttu.edu

**Abstract.** In the context of nonrelativistic quantum mechanics, Gaussian wavepacket solutions of the time-dependent Schrödinger equation provide useful physical insight. This is not the case for *relativistic* quantum mechanics, however, for which both the Klein-Gordon and Dirac wave equations result in strange and counterintuitive wavepacket behaviors, even for free-particle Gaussians. These behaviors include zitterbewegung and other interference effects. As a potential remedy, this paper explores a new trajectory-based formulation of quantum mechanics, in which the wavefunction plays no role [*Phys. Rev. X*, **4**, 040002 (2014)]. Quantum states are represented as ensembles of trajectories, whose mutual interaction is the source of all quantum effects observed in nature—suggesting a “many interacting worlds” interpretation. It is shown that the relativistic generalization of the trajectory-based formulation results in well-behaved free-particle Gaussian wavepacket solutions. In particular, probability density is positive and well-localized everywhere, and its spatial integral is conserved over time—in any inertial frame. Finally, the ensemble-averaged wavepacket motion is along a straight line path through spacetime. In this manner, the pathologies of the wave-based relativistic quantum theory, as applied to wavepacket propagation, are avoided.

## 1. Introduction

Quantum mechanics is generally regarded to be a theory based on wavefunctions [1, 2, 3]. The quantum wavefunction,  $\Psi$ , is thought to be the fundamental mathematical representation of the state of a quantum system. As such,  $\Psi$  has always enjoyed a hallowed status, despite much historical and ongoing disagreement about its precise interpretation or physical significance [4, 5, 6, 7, 8, 9, 10, 11]. Even “alternative” interpretations of quantum mechanics such as Bohmian mechanics [5, 6], which attribute physical reality to a “quantum trajectory,” nevertheless still adopt a hybrid ontology in practice, wherein it is a combination of both the wavefunction *and* the quantum trajectory, *together*, that specify the quantum state.

This article explores a fundamentally different kind of quantum theory, that makes no direct or indirect recourse to wavefunctions. It resembles Bohmian mechanics in that quantum trajectories are indeed employed. However, unlike Bohmian mechanics, *only* trajectories are used—the wave being replaced with a trajectory *ensemble*, which thereby represents the quantum state [12, 13, 14, 15, 16, 17, 18, 19, 20]. The trajectory ensemble is continuous, with each individual member trajectory labeled by the parameter  $C$ . The time evolution of the trajectory ensemble,  $x(t, C)$ , is governed by some partial differential equation (PDE) in  $(t, C)$  that replaces the usual time-independent Schrödinger equation governing the  $\Psi(t, x)$  evolution. All quantum

effects manifest as a dynamical interaction between neighboring trajectories in the ensemble—i.e., as partial derivatives in  $C$ . A new interpretation of quantum mechanics is thus also suggested by the new mathematics—what has come to be known as “many interacting worlds” [14, 19, 20].

Interpretations notwithstanding, in the nonrelativistic context described above, the wave-based and (continuous) trajectory-based mathematics are equivalent; thus, no new experimental predictions are proffered by the latter. On the other hand, a recent extension of the trajectory-based formulation to the *relativistic* quantum regime [21]—for single, massive, spin-zero, free particles, propagating on a flat Minkowski spacetime—does indeed provide new experimental predictions. However there are also other motivations for considering the relativistic extension of the trajectory theory. For example, the analogous wave-based relativistic quantum PDE for massive spin-zero particles—i.e. the Klein-Gordon equation—is riddled with foundational difficulties, when interpreted as a single-particle theory. Most problematically, the temporal component of the four-current is not positive over all spacetime, and therefore cannot be interpreted as a probability density [22, 23].

This “negative probability” issue is mostly resolved when one moves to spin-1/2 particles such as electrons, for which the Dirac equation is used to describe the relativistic quantum dynamics. On the other hand, both the Klein-Gordon and Dirac equations must contend with another difficulty, i.e. negative-energy solutions. Conceptually, one can address the negative-energy quantum states somewhat satisfactorily—in familiar terms involving positrons, the “Dirac sea,” etc. In practice, however, negative-energy states lead to highly undesirable outcomes, that manifest even in that simplest and most pedagogically useful of examples, the free-particle Gaussian wavepacket [24, 25]. By far the most famous of these undesired outcomes is *zitterbewegung*—rapid oscillations of the position expectation value over time, about a straight-line path through spacetime. However, this is but one of several “strange” behaviors observed in relativistic free-particle wavepacket dynamics, associated with interference between positive- and negative-energy components. These can be so severe that even 85+ years after they were first theoretically predicted, the physical origin and interpretation of these effects is still controversial, leaving even the standard probabilistic interpretation of the Dirac theory in doubt [24, 25]. A trajectory-based description may help substantially, in at least two different ways. First, it may admit an *analytical* wavepacket solution; according to one author, much of the remaining controversy “is all because there is no known analytical expression for a Dirac packet” [25]. Second, the relativistic quantum trajectory-based PDE *has* no negative-energy solutions, and is thereby possibly able to side-step the above difficulties, at least in principle. In any event, it is perhaps telling that true *zitterbewegung* has yet to be observed experimentally [25].

In this paper, we analyze the trajectory-based dynamical PDEs for spin-zero relativistic quantum particles, as derived in Ref. [21]. We also propagate those PDEs numerically, for various (initially) Gaussian wavepacket examples. We begin in Sec. 2, by introducing the dynamical PDEs for a relativistic quantum particle in  $(3 + 1)d$  spacetime. Then, in Sec. 3, we reduce the spacetime dimension to  $(1 + 1)d$  and derive dynamical equations specific to Gaussian wavepackets. Numerical solutions are also presented. The symmetry properties of the dynamical PDEs, together with their numerical solutions, are then investigated in Sec. 4, with respect to a set of scale transformations that preserves the equations of motion. The predicted scale invariance is verified both analytically and numerically. In this section, also, we examine the spacetime dependence of the spatial metric, which provides important dynamical information—e.g., as pertains to the relativistic restriction on wavepacket broadening.

Whereas an analytical solution may someday be tenable for the relativistic free-particle Gaussian wavepacket, at present we must rely on numerical solutions. Sec. 5 therefore addresses numerical issues, especially the issue of how to systematically characterize and improve the convergence accuracy of the numerical trajectory ensemble solutions. This is more difficult than for many standard numerical analyses, owing to the fact that the true boundary conditions are

unknown. As a consequence, numerical instabilities are sometimes encountered under certain conditions—although we provide one simple strategy for ameliorating this difficulty, involving nonuniform grids, which seems to work rather well.

The analysis up to this point in the paper pertains only to “stationary” Gaussian wavepackets, which remain centered at  $x = 0$  throughout time. In Sec. 6, we generalize everything for arbitrary moving free-particle Gaussian wavepackets, by simply applying Lorentz boosts to the stationary wavepacket solutions. In doing so, we confirm the Lorentz invariance of the dynamical PDEs and their numerical solutions, as well as the associated flux four-vectors. We also examine the probability density in both inertial frames, confirming that this quantity—the temporal component of the flux four-vector—is indeed positive throughout spacetime, and in all inertial frames. Finally, we confirm probability conservation by explicitly integrating the probability density over all space, and showing that the result is conserved over time—in any inertial frame. Thus, the trajectory-based treatment of relativistic free-particle Gaussian wavepackets does indeed appear to avoid the undesirable features of the corresponding wave-based approaches.

## 2. Dynamical equations in $(3 + 1)d$ spacetime

The following is a very brief overview of the derivation provided in Ref. [21], which should be consulted for further details. In the trajectory-based formulation for a single spin-free relativistic quantum particle in flat  $(3 + 1)d$  spacetime, a quantum state is represented as an ensemble of quantum trajectories,  $x^\alpha(X^\mu)$ . The *dependent* field variables are the inertial or extrinsic coordinates  $x^\alpha = (ct, \mathbf{x})$ , whereas the independent variables are the natural or intrinsic coordinates  $X^\mu = (c\lambda, \mathbf{C})$ . The quantity  $\lambda$  is a global time-like parameter called the “ensemble time,” whereas the three space-like  $\mathbf{C}$  coordinates label the individual quantum trajectories in the ensemble. Contours of the former, expressed in inertial coordinates, represent “simultaneity submanifolds”—i.e., global space-like-separated sets of events that occur simultaneously for the quantum particle. Contours of the latter—or rather, their mutual intersections—define the quantum trajectories themselves. These foliate spacetime, and may be interpreted as a continuous spectrum of “worlds,” in each of which resides a single “copy” of the particle. Both  $\lambda$  and  $\mathbf{C}$  may be separately reparametrized, in arbitrary fashion.

We denote the metric tensor of the natural coordinate system as  $g^{\mu\nu}$ , and that of the inertial coordinates as  $\eta^{\alpha\beta}$ . These are related via the transformation,

$$g_{\mu\nu} = \eta_{\alpha\beta} \frac{\partial x^\alpha}{\partial X^\mu} \frac{\partial x^\beta}{\partial X^\nu}. \quad (1)$$

In matrix form, the inertial metric tensor is the familiar  $\tilde{\eta} = \text{diag}(-1, 1, 1, 1)$ . For the natural coordinates, we impose local orthogonality between infinitesimal displacements in  $\lambda$  and  $\mathbf{C}$ . This results in a block-diagonal metric tensor, i.e.

$$\tilde{g} = \begin{pmatrix} g_{00} & 0 \\ 0 & \tilde{\gamma} \end{pmatrix}, \quad (2)$$

where the “spatial metric”  $\tilde{\gamma}$  denotes the  $3 \times 3$  spatial block of  $\tilde{g}$ . We further define

$$g = \det \tilde{g} \quad ; \quad \gamma = \det \tilde{\gamma}. \quad (3)$$

Finally, we note that  $g_{00} = -(d\tau/d\lambda)^2$ , where  $\tau$  is the usual proper time, defined via

$$d\tau^2 = -\frac{1}{c^2} \eta_{\alpha\beta} dx^\alpha dx^\beta. \quad (4)$$

Probability conservation along individual quantum trajectories is presumed [21], as a result of which the spatial scalar probability density on  $\mathbf{C}$ -space,  $f(\mathbf{C})$ , must be independent of  $\lambda$ . In addition to this scalar quantity, there is also the *flux four-vector*,

$$j^\mu = f(\mathbf{C}) \frac{dX^\mu}{d\lambda} = (cf(\mathbf{C}), 0, 0, 0), \quad (5)$$

which transforms as a contravariant vector density of weight  $W = -1$ . Due to a fortuitous cancellation of Christoffel symbols,  $j^\mu$  satisfies the following covariant continuity equation,

$$\partial_\mu j^\mu = 0, \quad (6)$$

in *all* coordinate frames. In an inertial frame, in particular, this leads to the familiar integrated form of probability conservation,

$$\int j^0(x^\alpha) d^3x = \text{const.} \quad (7)$$

It is noteworthy that  $j^0$  can be interpreted as a true *probability* density (apart from a scaling factor), as in nonrelativistic quantum mechanics. The analogous Klein-Gordon  $j^0$  quantity, for example, can change sign, and must therefore be interpreted as a *charge* density [22, 23].

In addition to its usual probabilistic role,  $f(\mathbf{C})$  also plays an indirect *dynamical* role in the quantum trajectory theory. The quantum potential  $Q$  and the quantum force  $f^\alpha$  are given by

$$Q = -\frac{\hbar^2}{2m} \gamma^{-1/4} f^{-1/2} \frac{\partial}{\partial C^i} \left[ \gamma^{1/2} \gamma^{ij} \frac{\partial}{\partial C^j} (f^{1/2} \gamma^{-1/4}) \right], \quad (8)$$

$$f^\alpha = -\eta^{\alpha\beta} \frac{\partial C^i}{\partial x^\beta} \frac{\partial Q}{\partial C^i} = -\frac{\partial x^\alpha}{\partial C^i} \gamma^{ij} \frac{\partial Q}{\partial C^j}, \quad (9)$$

where  $\gamma^{ij}$  is the matrix form of  $\tilde{\gamma}^{-1}$ . The above equations are valid for any parametrization of  $\lambda$  and  $\mathbf{C}$ . On the other hand, we can make a special choice for  $\lambda$ , known as the “ensemble proper time,”  $\mathcal{T}$ , which reduces to  $\tau$  when  $Q = 0$ . More generally [21], the relation is

$$\frac{d\tau}{d\mathcal{T}} = \exp\left(-\frac{Q}{mc^2}\right). \quad (10)$$

This leads, finally, to the dynamical equations of motion for a free particle:

$$\frac{\partial^2 x^\alpha}{\partial \mathcal{T}^2} = \exp\left(\frac{-2Q}{mc^2}\right) \frac{f^\alpha}{m} - \frac{1}{mc^2} \frac{\partial Q}{\partial \mathcal{T}} \frac{\partial x^\alpha}{\partial \mathcal{T}}. \quad (11)$$

Solving Eq. (11) requires specification of the initial conditions,  $x_0^\alpha = x^\alpha(0, \mathbf{C})$  and  $(\partial x^\alpha / \mathcal{T})(0, \mathbf{C})$ .

Note that Eq. (11) is second order in  $\mathcal{T}$  and fourth order in  $\mathbf{C}$ —in exact analogy with the time and space orders of the Schrödinger PDE (the order doubling is due to the fact that the field quantity is in this case real- rather than complex-valued). Thus, *natural* time and *natural* space are not treated on an equal footing in this relativistic picture—but then again, neither should they be. In contrast, the *inertial* coordinates,  $x^\alpha$  are treated equally, in the sense that Eq. (11) is Lorentz-invariant. In this manner—i.e., by separating natural from inertial coordinates—we are able to avoid the relativistic quantum “paradox” that, for example, led Dirac to consider multiple wave components. Moreover, the negative energy solutions that one finds with Klein-Gordon [22, 26, 27] or Dirac [22, 26, 27] also go away, because one finds that positive-negative pairs of wavefunction solutions correspond to a single trajectory ensemble solution  $x^\alpha(X^\mu)$  [21].

### 3. Gaussian wavepacket solutions in $(1+1)d$ spacetime

Some analytical and numerical solutions of Eq. (11) are provided in Ref. [21], for  $(1+1)d$  spacetime. In this reduced-dimensional context, there is but a single inertial (natural) spatial coordinate,  $x = x^1$  ( $C = C^1$ ), and the dynamical equations simplify as a consequence of

$$\frac{1}{\gamma^{ij}} = \gamma_{ij} = \gamma = \left( \frac{\partial x}{\partial C} \right)^2 - c^2 \left( \frac{\partial t}{\partial C} \right)^2. \quad (12)$$

For the remainder of this article, we will focus on  $(1+1)d$  spacetime, and specifically on the free particle propagation of the relativistic Gaussian wavepacket. In nonrelativistic quantum mechanics, the Gaussian wavepacket is well known to disperse while moving in a straight line—yet retains a perfect Gaussian shape at all times [2]. The wavepacket spreading is therefore linear. This behavior cannot also characterize the relativistic regime, for it would imply the existence of faster-than-light quantum trajectories in the Gaussian tails, which are precluded by the  $(1+1)d$  Eq. (11). At best, the relativistic wavepacket can be truly Gaussian at a single time only. Moreover, one has to resolve which “time” is being referred to, i.e.  $\mathcal{T}$  or  $t$ .

Both issues are resolved by considering coherent-state or minimum-uncertainty Gaussians, which exhibit uniform flux/velocity throughout  $x$ . All nonrelativistic free-particle Gaussian wavepackets evolve into a coherent state at exactly one point in time during their lifecycles. By setting this time equal to zero, and transforming to a frame in which the uniform velocity is zero, all quantum trajectories in the ensemble become instantaneously stationary. The relativistic and nonrelativistic descriptions must therefore agree in that initial instant. In particular, the  $t = 0$  and  $\mathcal{T} = 0$  initial conditions become identical. Our ansatz for a free-particle relativistic Gaussian wavepacket therefore becomes a solution of  $(1+1)d$  Eq. (11) whose initial conditions satisfy:

$$t_0(C) = 0 \quad ; \quad x_0(C) = C \quad ; \quad \frac{\partial x}{\partial \mathcal{T}}(0, C) = 0, \quad \text{with } f(C) = \exp(-aC^2). \quad (13)$$

Note that Eq. (13) implies a specific parametrization for  $C$ —i.e., for any given trajectory,  $C$  is the initial  $x$  value,  $x_0$  [14, 21]. Likewise, our earlier specification of the natural time coordinate,  $\lambda = \mathcal{T}$ , implies the following as the one remaining initial condition:

$$\frac{\partial t}{\partial \mathcal{T}}(0, C) = \exp\left[-\frac{Q_0(C)}{mc^2}\right] = \exp\left[\frac{1}{2}\left(\frac{\hbar}{mc}\right)^2 (a^2 C^2 - a)\right]. \quad (14)$$

In Eq. (14) above,  $Q_0(C) = Q(0, C)$  is the initial quantum potential. More generally, Eqs. (8) and (9) reduce to the following, for  $(1+1)d$  spacetime with the  $f(\mathbf{C})$  choice of Eq. (13):

$$Q = -\frac{\hbar^2}{2m} \frac{e^{\frac{1}{2}aC^2}}{\gamma^{1/4}} \frac{\partial}{\partial C} \left[ \frac{1}{\gamma^{1/2}} \frac{\partial}{\partial C} \left( e^{-\frac{1}{2}aC^2} \gamma^{-1/4} \right) \right]; \quad (15)$$

$$f^0 = -\frac{c}{\gamma} \frac{\partial t}{\partial C} \frac{\partial Q}{\partial C} \quad ; \quad f^1 = -\frac{1}{\gamma} \frac{\partial x}{\partial C} \frac{\partial Q}{\partial C}. \quad (16)$$

The resultant dynamical equations become

$$\begin{aligned} -\frac{1}{m} \frac{1}{\gamma} \frac{\partial t}{\partial C} \frac{\partial Q}{\partial C} &= \exp\left(\frac{Q}{mc^2}\right) \frac{\partial}{\partial \mathcal{T}} \left[ \exp\left(\frac{Q}{mc^2}\right) \frac{\partial t}{\partial \mathcal{T}} \right], \\ -\frac{1}{m} \frac{1}{\gamma} \frac{\partial x}{\partial C} \frac{\partial Q}{\partial C} &= \exp\left(\frac{Q}{mc^2}\right) \frac{\partial}{\partial \mathcal{T}} \left[ \exp\left(\frac{Q}{mc^2}\right) \frac{\partial x}{\partial \mathcal{T}} \right]. \end{aligned} \quad (17)$$

To date, analytical solutions of Eq. (17) for  $t(\mathcal{T}, C)$  and  $x(\mathcal{T}, C)$  have eluded us. However, we have obtained numerical solutions, for  $a = 1/2$ ,  $\hbar = m = 1$ , and various values of the speed

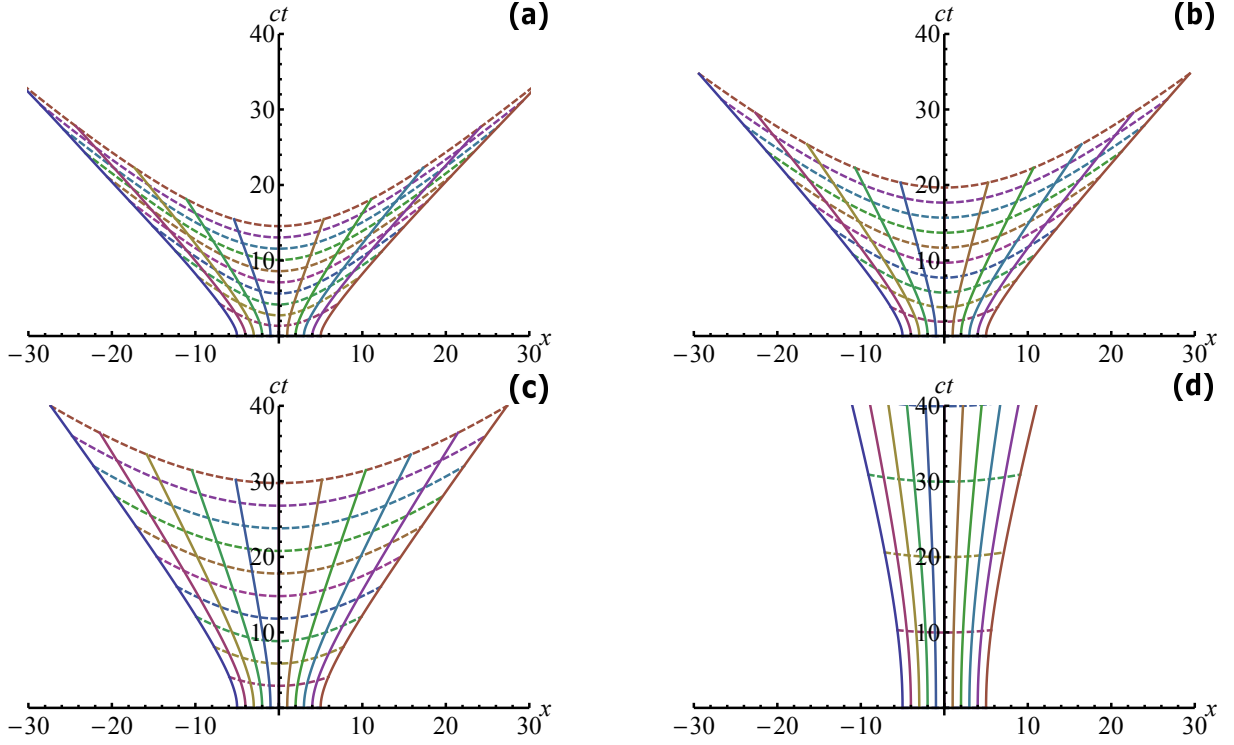


**Figure 1.** Quantum trajectories (solid curves) and simultaneity submanifolds (dashed curves) for the relativistic free-particle Gaussian wavepacket of Eq. (13), for  $a = 1/2$ ,  $\hbar = m = 1$ , and several choices of the speed of light,  $c$ : (a)  $c = 1.5$ ; (b)  $c = 2.0$ ; (c)  $c = 3.0$ ; (d)  $c = 10$ .

of light  $c$ , as presented in Fig. 1. Wavepacket spreading is evident, as in the nonrelativistic case. The quantum trajectories approach the light cone faster in the ultrarelativistic limit of small  $c$ , as expected. The simultaneity submanifolds also become increasingly distorted in this limit, whereas in the nonrelativistic (large  $c$ ) limit, they approach horizontal lines (i.e., contours of  $t$ ).

#### 4. Scale invariance of the dynamical solutions, and the spatial metric

The PDE of Eq. (17) governs the time evolution of the quantum trajectory ensemble for the relativistic free-particle Gaussian wavepacket. Rescaling the system parameters of this PDE alters its solutions. However, it is possible to rescale the parameters and dynamical variables together, in such a way that the solutions remain invariant. Consider the double scale transformation defined in terms of the two parameters,  $\zeta$  and  $\eta$ , with  $\zeta$  associated with  $c$ , and  $\eta$  with the independent and dependent variables, as follows:

$$c \rightarrow \zeta c \quad ; \quad X^\mu \rightarrow \eta X^\mu \quad ; \quad x^\alpha \rightarrow \eta x^\alpha. \quad (18)$$

$$\mathcal{T} \rightarrow \frac{\eta}{\zeta} \mathcal{T} \quad ; \quad C \rightarrow \eta C \quad ; \quad t \rightarrow \frac{\eta}{\zeta} t \quad ; \quad x \rightarrow \eta x. \quad (19)$$

For the quantum trajectory ensemble solution to remain invariant, Eq. (13) implies that  $f(C)$  must also remain invariant. Under the rescaling  $C \rightarrow \eta C$ , this requires  $a \rightarrow (1/\eta^2)a$ . More generally, the invariance of the solution under  $C \rightarrow \eta C$  rescaling implies:

$$\gamma \rightarrow \gamma \text{ from Eqs. (12) and (19)} \quad ; \quad \frac{Q}{mc^2} \rightarrow \frac{Q}{mc^2} \text{ from Eq. (17)} \quad (20)$$

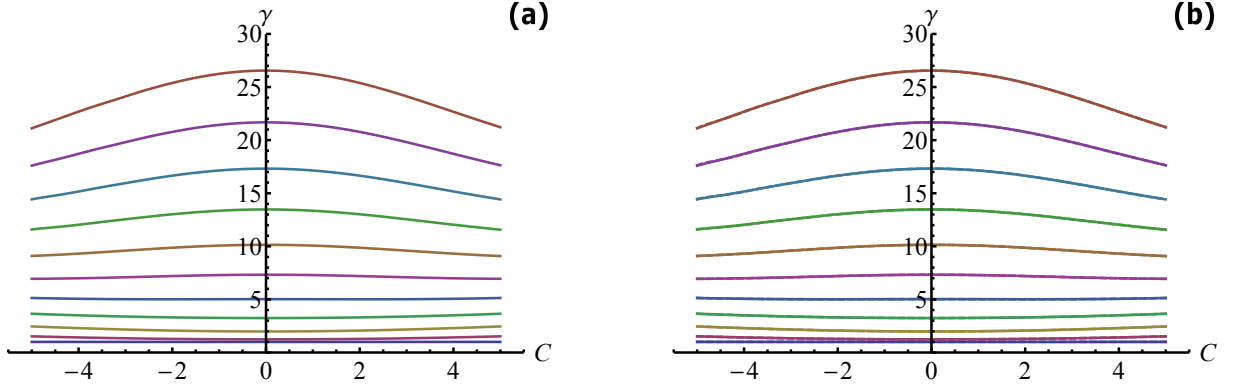


**Figure 2.** Spatial metric  $\gamma(\mathcal{T}, C)$  for  $(1+1)d$  relativistic free-particle Gaussian wavepackets. Each curve represents  $\gamma(C)$  for fixed  $\mathcal{T} = \{0, 1, 2, \dots, 10\}$ , with increasing  $\mathcal{T}$  values corresponding to increasing  $\gamma$ : (a) ( $a = 1/2, \hbar = 1, c = 3$ ) solution; (b) comparison between ( $a = 1/2, \hbar = 1, c = 3$ ) and ( $a = 1/5, \hbar = 5\sqrt{10}/3, c = 10$ ) solutions, which are numerically nearly indistinguishable.

$$\left(\frac{\hbar}{mc}\right)^2 \rightarrow \eta^2 \left(\frac{\hbar}{mc}\right)^2 \quad \text{from Eqs. (8) and (20).} \quad (21)$$

Now we consider the invariance of the solution under  $c \rightarrow \zeta c$ , which implies:

$$\frac{\hbar}{m} \rightarrow \eta \zeta \left(\frac{\hbar}{m}\right) \quad \text{from Eq. (21)} \quad ; \quad \frac{Q}{m} \rightarrow \zeta^2 \frac{Q}{m} \quad \text{from Eq. (20)} \quad (22)$$

$$\frac{f^\alpha}{m} \rightarrow \frac{\zeta^2}{\eta} \left(\frac{f^\alpha}{m}\right) \quad \text{from Eqs. (16), (19) and (22).} \quad (23)$$

Finally, we examine the rescaling of Eq. (17) directly. Under the simultaneous rescaling  $C \rightarrow \eta C$  and  $c \rightarrow \zeta c$ , the left hand side of Eq. (17) is found to rescale as  $\zeta^2/\eta$ . The right hand side also rescales as  $\zeta^2/\eta$ —thus implying scale invariance for the free-particle Gaussian wavepacket evolution. More generally, similar arguments are also found to hold for Eq. (11). The scale invariance has also been verified numerically. In Fig. 2, we compare  $\gamma(\mathcal{T}, C)$  for the ( $a = 1/2, \hbar = m = 1, c = 3$ ) Gaussian wavepacket solution vs. that for ( $a = 1/5, \hbar = 5\sqrt{10}/3, m = 1, c = 10$ )—corresponding to the ( $\zeta = 10/3, \eta = \sqrt{5/2}$ ) rescaling. We observe that all of the fixed- $\mathcal{T}$   $\gamma(C)$  curves are numerically nearly indistinguishable.

Since  $\gamma$  in fact represents the spatial metric, Fig. 2 provides useful insight into the wavepacket dynamics. The primary feature evident in the plots is that the  $\gamma(C)$  curves increase in magnitude with increasing  $\mathcal{T}$ —an indication of wavepacket broadening. Note, however, that this increase is not uniform across  $C$ —i.e., the curves are not horizontal lines. If they were, this would imply preservation of the Gaussian form over time, which only occurs in the nonrelativistic limit. Conversely, the curvature or bowing of these curves—which for this example, is seen to be rather pronounced—is an indication of relativistic quantum dynamical effects.

Another interesting feature may also be observed in Fig. 2, which is that the direction of the curvature changes over time. The early curves bow upward, whereas at later times, the curves bow downward. This can be explained as a competition between the dynamical influences of  $Q$  and  $f^\alpha$ . At early times, all trajectories are “moving” in unison; their acceleration has not yet had a chance to manifest as a fanning out of velocities. However, even at  $\mathcal{T} = 0$ , the local proper time evolves at a higher rate towards the exterior fringes of the ensemble (i.e., towards

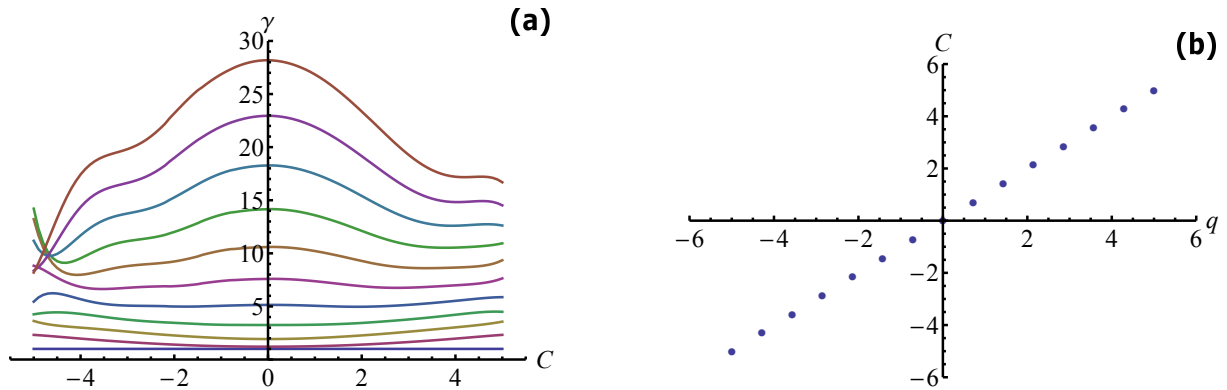


**Figure 3.** Calculations with a uniformly-spaced  $C$  grid: (a) numerically computed  $\gamma(\mathcal{T}, C)$ , as per Fig. 2, but for  $c = 1.5$ ; (b) the  $N_g = 15$  grid points themselves, uniformly spaced over  $-5 \leq C \leq 5$ .

larger  $|C|$ )—in accord with the relativistic quantum *time compression* effect [21]. The early simultaneity submanifolds thus curve away from the  $x$  axis, resulting in larger intervals between nearby trajectories that lie further from  $C=0$ —and thus, in upward-bowing  $\gamma(C)$  curves. Over time, acceleration gives rise to trajectory fanout, as discussed. However, as the velocities of the exterior trajectories reach the order of the speed of light, further broadening of the wavepacket is relativistically hindered, and so the resultant  $\gamma(C)$  curves bow downward, rather than upward.

## 5. Numerical details

From a numerical standpoint, the solution of Eq. (17) offers important advantages over both conventional,  $x$ -grid-based Crank-Nicholson propagation of  $\Psi$ , and traditional quantum trajectory methods [28]. Briefly, one has the simultaneous advantages of *both* a regular grid (in  $C$ ) *and* probability-conserving trajectories (in  $x$ ) [14]. There are nevertheless some nontrivial numerical issues, stemming from the fact that the true boundary conditions are unknown—unlike for  $\Psi$  propagation, for which Dirichlet boundary conditions are in effect. In practice, as a result of the small asymptotic density  $f(C)$ , the less significant boundary regions seem to have very little effect on the far more important interior. Consequently, one can choose any reasonable boundary condition—or none at all, as is the case with most of our *Mathematica* calculations (performed using **NDSolve**)—and still obtain excellent results. On the other hand, there are also situations when this boundary condition issue can cause numerical instabilities. This is an ongoing area of investigation, though we discuss one simple example and remedy here.

For the present Gaussian wavepacket calculations, errors and instabilities tend to increase when the numerical grid is extended over a larger  $C$  domain, and also in the ultrarelativistic limit. Figure 3 presents  $\gamma(C)$  curves for the  $c = 1.5$  example of Fig. 1(a), as computed using a simple uniformly-spaced  $C$  grid of  $N_g = 15$  points, over the domain  $-C_{\max} \leq C \leq C_{\max}$ , with  $C_{\max} = 5$ . The lack of symmetry, curve-crossing, and sharp changes are all evidence of numerical inaccuracy in the boundary regions, although the interior trajectories where probability is significant are still fairly accurate. Simply increasing the number of grid points, however, without changing the  $C$  domain, does not lead to improved accuracy, and actually makes the boundary behavior worse. The same is true if  $C_{\max}$  is increased, using the same grid density.

Based on these observations, we instead adopt a *nonuniform*  $C$  grid, wherein a higher density of grid points is used in the more important interior region. This is achieved via the map,

$$C(q) = A \tanh^{-1}(\beta q), \quad (24)$$



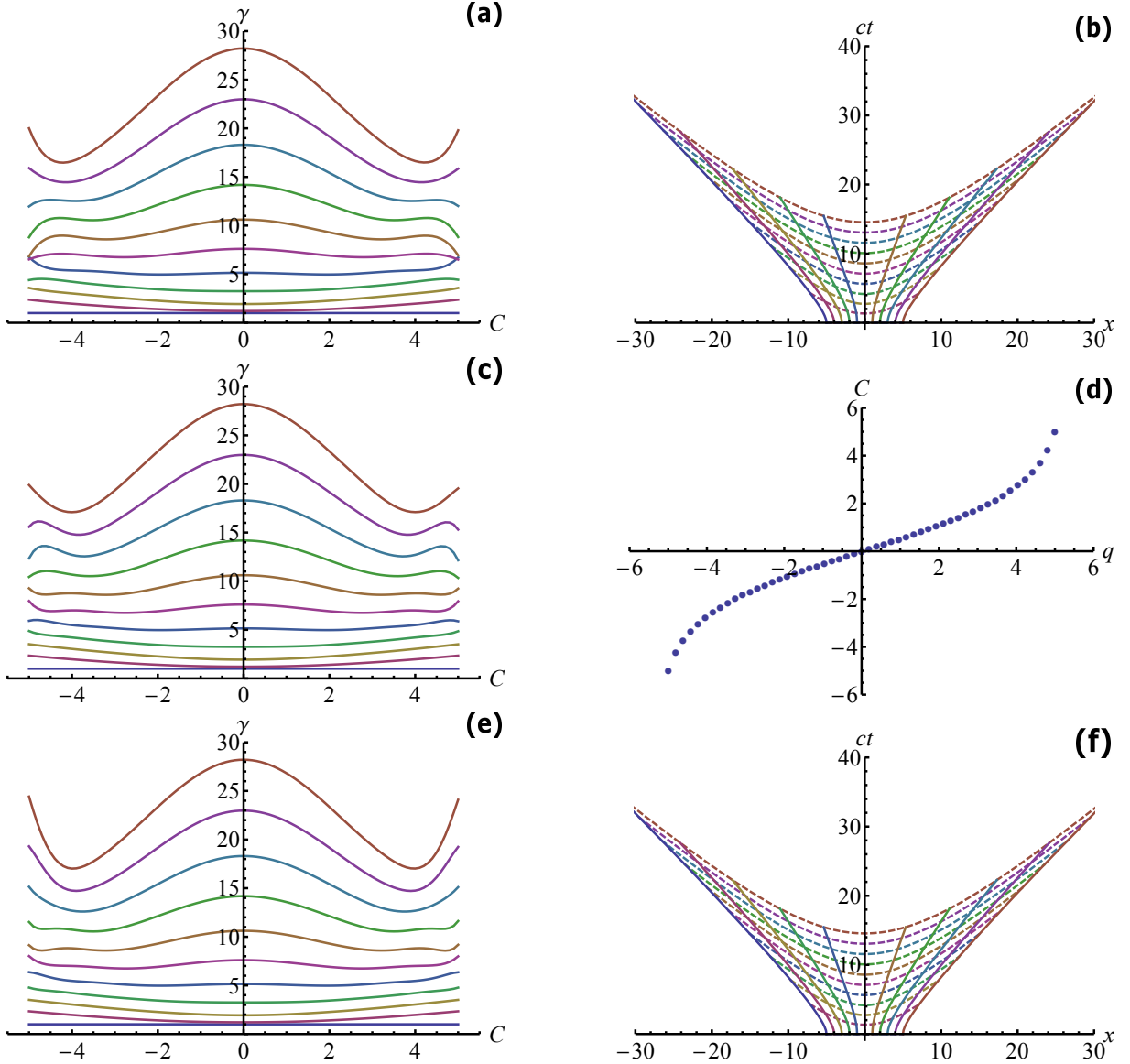


**Figure 4.** Calculations with nonuniform  $C$  grids:  $N_g = 23$  [(a) and (b)];  $N_g = 53$  [(c) and (d)];  $N_g = 93$  [(e) and (f)]. Numerical  $\gamma(\mathcal{T}, C)$  curves [(a), (c), and (e)], as per Fig. 2] exhibit obvious discrepancies in the boundary regions, but are very accurate in the interior. Quantum trajectories [(b) and (f)] are nearly indistinguishable. The  $N_g = 53$  grid is presented in (d).

where grid points are now uniformly distributed over  $-q_{\max} \leq q \leq q_{\max}$ . The quantity  $A = C_{\max} / \tanh^{-1}(\beta q_{\max})$ , and  $\beta$  is the nonuniformity parameter. The nonuniform grid greatly improves asymptotic behavior, thereby allowing for higher grid densities and more accurate calculations in the interior.

For the above  $c = 1.5$  example, the choice ( $q_{\max} = 5, C_{\max} = 5, \beta = 0.19$ ) enables stable, accurate calculations to be performed up to  $N_g = 93$  grid points, as depicted in Fig. 4. Although numerical discrepancies in the boundary regions of the Fig. 4 curves are still evident, we emphasize that the wavepacket as a whole is *extremely* well-converged. This is evident in Fig. 5, which depicts the *probability-weighted* errors as a function of  $C$  and  $\mathcal{T}$ , for two different nonuniform grid calculations, of sizes  $N_g = 53$  and  $N_g = 83$ , respectively. The larger grid size

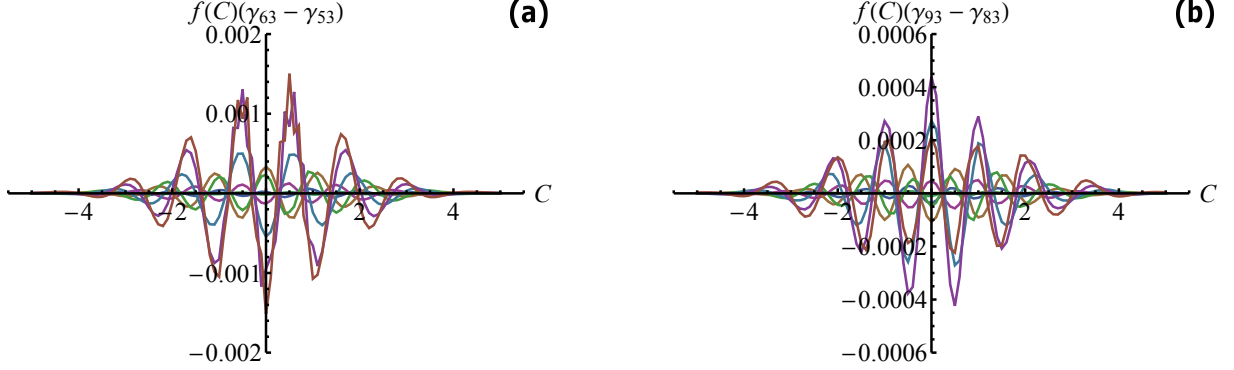


**Figure 5.** Probability-weighted convergence errors for nonuniform  $C$  grid calculations of  $\gamma(\mathcal{T}, C)$ , as per Fig. 2: (a) for  $N_g = 53$ ; (b) for  $N_g = 83$ . In each case, the error is defined relative to a slightly larger calculation, as  $f(C)(\gamma_{N_g+10} - \gamma_{N_g})$ . Numerical errors are substantially smaller for the larger grid, but in both cases the largest probability-weighted errors are in the interior.

of the latter leads to substantial improvements in accuracy in the interior region. This is where the largest errors are to be found, in the probabilistic sense, although they are still quite small.

## 6. Probability conservation and Lorentz-boosted inertial frames

In Secs. 3 and 5, we considered only free-particle Gaussian wavepackets which, at the initial time  $\mathcal{T} = 0$ , comprise a stationary coherent state (i.e.,  $\partial x / \partial \mathcal{T}|_{\mathcal{T}=0} = 0$ ) that is centered at the origin [i.e.,  $x_0(C = 0) = 0$ ]. More generally, we wish to consider *nonstationary* wavepackets, for which the wavepacket center moves along an arbitrary (time-like) straight line. The most general possible relativistic free-particle Gaussian wavepacket solutions may be obtained from the stationary solutions through an arbitrary combination of: (a) translation in  $t$ ; (b) translation in  $x$ ; (c) Lorentz boost. Whereas (a) and (b) are trivial and will not be considered further, (c) serves as an explicit check on the Lorentz-invariance of the dynamical equations (despite the different PDE orders in  $\mathcal{T}$  and  $C$ ), as well as the inertial coordinate probability conservation laws, as discussed in Sec. 2.

Let  $S$  denote the inertial frame of reference  $(ct, x)$ , in which the free-particle Gaussian wavepacket adopts the “stationary” form, in the sense described above. Let  $S'_{[v]}$  denote a new inertial frame,  $(ct', x')$ , obtained from  $S$  via application of the Lorentz boost corresponding to the positive velocity  $v > 0$ . In this manner, we obtain a new set of solutions,  $\{x'^{\alpha}_{[v]}(X^{\mu})\}$ , each of which describes a quantum particle moving toward the negative  $x'$ -direction with ensemble-averaged velocity  $-v$ . For each boosted trajectory ensemble solution  $x'^{\alpha}_{[v]}(X^{\mu})$ , the corresponding flux “four”-vector  $j'^{\alpha}(x')$  can be easily obtained in the boosted frame  $S'_{[v]}$ .

It is of interest to verify the conservation of probability [Eq. (7)] and covariant continuity relation [Eq. (6)] of Sec. 2 numerically, in both stationary and boosted inertial frames. We do so for the stationary frame as follows. The stationary inertial flux four-vector is expressed as [21],

$$j^{\alpha}(x) = \frac{f(C)}{\sqrt{\gamma}} \frac{dx^{\alpha}}{d\tau} = \frac{e^{-aC^2}}{\sqrt{\gamma}} \frac{dx^{\alpha}}{d\tau}. \quad (25)$$

We obtain the probability density and flux, respectively, as follows:

$$j^0(ct, x) = c \frac{f(C)}{\sqrt{\gamma}} \frac{dt}{d\tau} \quad ; \quad j^1(ct, x) = \frac{f(C)}{\sqrt{\gamma}} \frac{dx}{d\tau}, \quad (26)$$

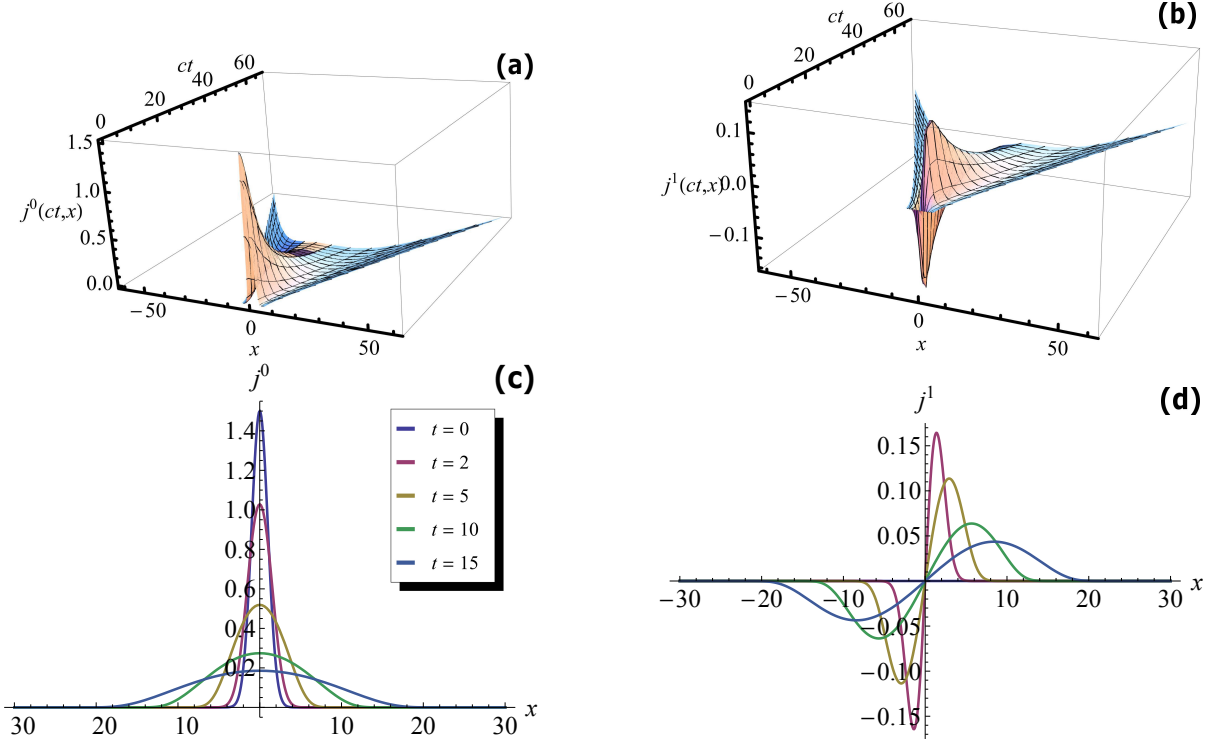


**Figure 6.** Flux four-vector for the relativistic free-particle Gaussian wavepacket for  $c = 1.5$ : (a) three-dimensional plot of  $j^0(ct, x)$ ; (b) three-dimensional plot of  $j^1(ct, x)$ ; (c) time slice plots of  $j^0(ct, x)$ ; (d) time slice plots of  $j^1(ct, x)$ . The time slices are for  $t = \{0, 2, 5, 10, 15\}$ .

where

$$\frac{dt}{d\tau} = \frac{1}{\sqrt{1 - \frac{1}{c^2} \left(\frac{dx}{dt}\right)^2}} \quad ; \quad \frac{dx}{d\tau} = \frac{\frac{dx}{dt}}{\sqrt{1 - \frac{1}{c^2} \left(\frac{dx}{dt}\right)^2}}. \quad (27)$$

To obtain  $j^\alpha(ct, x)$  numerically, we start with the numerical quantum trajectory ensemble solution,  $x^\alpha(X^\mu) = (ct(\mathcal{T}, C), x(\mathcal{T}, C))$ . From the latter we obtain  $dx/dt$  everywhere via

$$\frac{dx}{dt} = \left. \frac{\partial x}{\partial \mathcal{T}} \right|_C \left( \left. \frac{\partial t}{\partial \mathcal{T}} \right|_C \right)^{-1}. \quad (28)$$

Substituting Eq. (28) into Eq. (27), and again into Eq. (26), we obtain numerical results for  $j^0(ct, x)$  and  $j^1(ct, x)$ . These are presented in Fig. 6, for the  $c = 1.5$  example.

In Fig. 6(a) and (c), we observe that  $j^0(ct, x) > 0$  for all  $(ct, x)$ —i.e., the probability density remains positive always. We also observe substantial broadening of the wavepacket over time. However, the initial Gaussian shape is also substantially distorted over time, with the fringe trajectories “bunching up” as they approach the speed of light (Sec. 4). As for the flux,  $j^1(ct, x)$ , it is always odd in  $x$ , being positive for  $x > 0$  and negative for  $x < 0$  (for  $t \geq 0$ ). This also reflects wavepacket broadening—i.e., trajectories to the right of  $x = 0$  spread to the right, whereas those to the left spread to the left. Although the trajectory speeds increase monotonically with increasing  $|C|$ , the flux reaches a maximum and then decays, owing to the probability weighting. Finally, according to the  $(1+1)d$  Eq. (7), the areas under each of the  $j^0(x)$  curves in Fig. 6(c) should be constant, if probability is conserved. Numerical integration for each of the sixteen  $t$

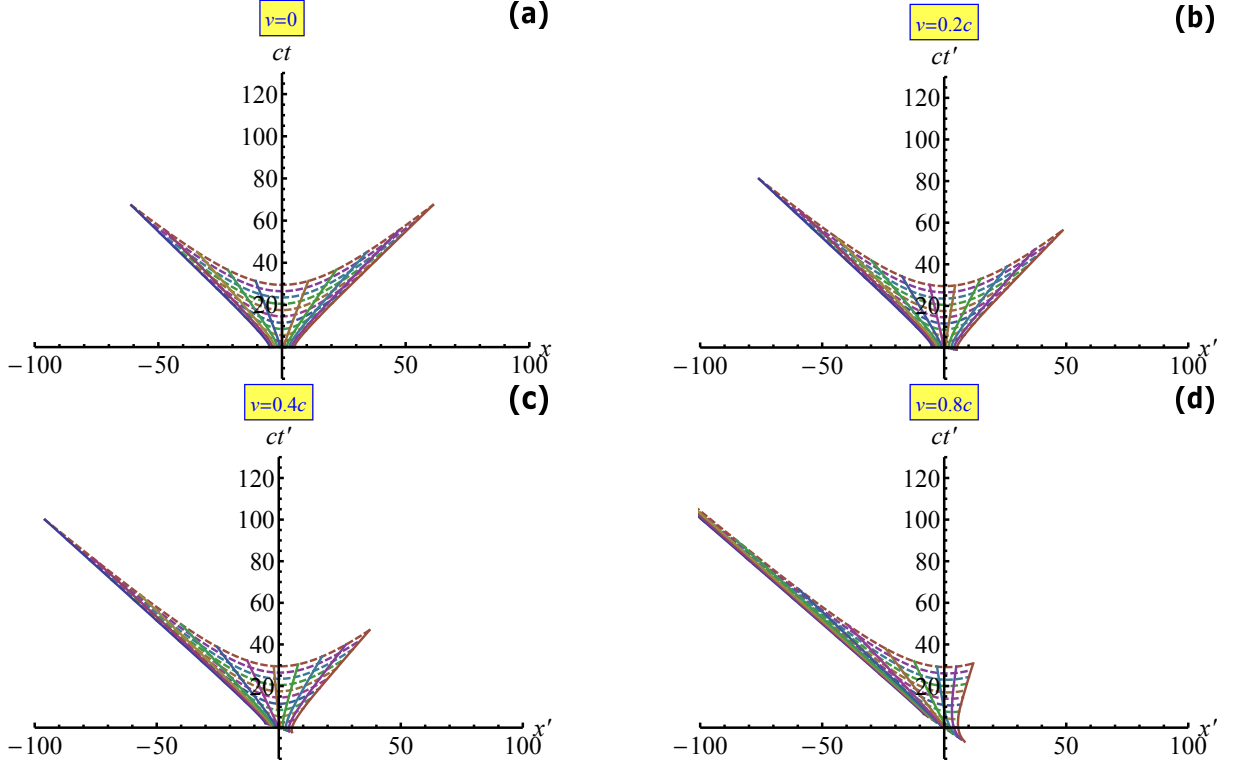


**Figure 7.** Quantum trajectories (solid curves) and simultaneity submanifolds (dashed curves) for the relativistic free-particle Gaussian wavepacket for  $c = 1.5$ , in various stationary and Lorentz-boosted frames: (a)  $v = 0.0c$ ; (b)  $v = 0.2c$ , (c)  $v = 0.4c$ ; (d)  $v = 0.8c$ .

values,  $t = \{0, 1, 2, \dots, 15\}$ , results in a near-constant value of 3.7615, with an RMS error of only 0.0011.

In the Lorentz-boosted frame  $S'_{[v]}$ , we denote the flux four-vector as  $j'^\alpha(ct', x')$ . Being a true Lorentz-invariant vector, this quantity must transform as does  $x^\alpha$ —i.e., as

$$x'^\alpha = \Lambda^\alpha_\delta x^\delta \quad ; \quad j'^\alpha(ct', x') = \Lambda^\alpha_\delta j^\delta(ct, x), \quad (29)$$

where the rank-2 boost tensor  $\Lambda^\alpha_\delta$  can be expressed in terms of the parameter  $\beta = v/c$  as

$$\Lambda^\alpha_\delta = \begin{pmatrix} \frac{1}{\sqrt{1-\beta^2}} & \frac{-\beta}{\sqrt{1-\beta^2}} \\ \frac{-\beta}{\sqrt{1-\beta^2}} & \frac{1}{\sqrt{1-\beta^2}} \end{pmatrix}, \quad (30)$$

in the usual manner.

In the Lorentz-boosted frame  $S'_{[v]}$ , a *different* probability conservation law than Eq. (7) must hold, namely,

$$\int j'^0(ct', x') dx' = \text{const.} \quad (31)$$

Once again, we will verify numerically that the Eq. (31) probability conservation law is indeed satisfied. First, however, we obtain the trajectory ensemble solution,  $x'^\alpha(X^\mu)$ , by Lorentz-boosting  $x^\alpha(X^\mu)$  (dropping the '[v]' subscript). Then, we apply a second Lorentz boost to the dependent variables  $j^\alpha = (j^0, j^1)$ , to obtain the desired functions  $j'^0(ct', x')$  and  $j'^1(ct', x')$ .

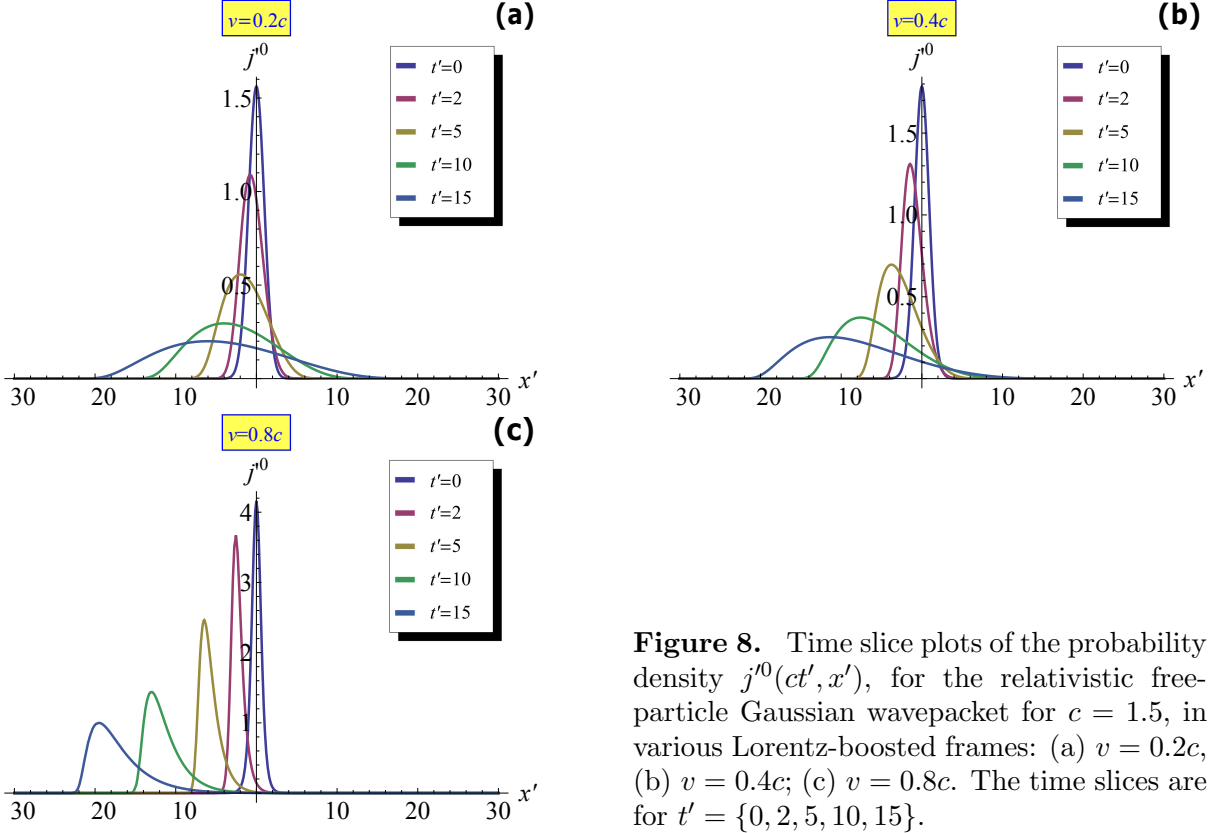


**Figure 8.** Time slice plots of the probability density  $j^0(ct', x')$ , for the relativistic free-particle Gaussian wavepacket for  $c = 1.5$ , in various Lorentz-boosted frames: (a)  $v = 0.2c$ , (b)  $v = 0.4c$ ; (c)  $v = 0.8c$ . The time slices are for  $t' = \{0, 2, 5, 10, 15\}$ .

In Fig. 7, we depict the quantum trajectories and simultaneity submanifolds in the stationary frame  $S$ , and in several boosted frames  $S'_{[v]}$  for  $v = 0.2c$ ,  $v = 0.4c$  and  $v = 0.8c$ . The boosted quantum trajectories do indeed move generally to the left, increasingly so for increasing  $v$ . The trajectory ensemble is no longer symmetric in  $x'$ , but it is symmetric under  $(ct', x') \rightarrow (-ct', -x')$ , as would be expected from the nonrelativistic case. Figure 8 depicts  $j^0(ct', x')$ , plotted as a function of  $x'$  for various time slices  $t'$ , for  $v = 0.2c$ ,  $v = 0.4c$  and  $v = 0.8c$ . In all cases, the motion of the wavepacket to the left over time is evident, as is wavepacket broadening. We also observe a “bunching” distortion of the Gaussian form in the wavepacket fringes, similar to that evident in Fig. 6(c) for the stationary case. Here, however, for all  $t' \neq 0$ , the wavepacket is not even symmetric about its center—unlike both the travelling nonrelativistic Gaussian wavepacket, and the stationary relativistic example discussed previously. The reason is clear: due to the velocity bias in the ensemble, trajectories to the left of the wavepacket center experience much more pronounced bunching than those to the right—which may not even bunch at all, if the region of significant probability is always moving to the left over the time scale of interest.

Finally, we consider conservation of probability. First, note that according to Figure 8,  $j^0(ct', x') \geq 0$  for all  $(ct', x')$ —thus justifying our interpretation of this quantity as a probability density. Also, once again, for Eq. (31) to be satisfied, the areas under each of the curves in Fig. 8 must be the same, for a given  $v$  value. Via numerical integration, this is indeed found to be the case. Specifically: for  $v = 0.2c$ , the integration for each curve yields 3.8369, with an RMS error of 0.0008; for  $v = 0.4c$ , the integration for each curve yields 4.1029, with an RMS error of 0.0009; for  $v = 0.8c$ , the integration for each curve yields 6.2704, with an RMS error of 0.0097. Thus, we conclude that conservation of probability as per Eq. (31) holds in all Lorentz-boosted frames,  $S'_{[v]}$ , and therefore for all relativistic free-particle Gaussian wavepackets.

## 7. Summary and Conclusions

In this paper, we analyze the dynamical equations for a single, spin-zero relativistic quantum particle, based on a recently-derived trajectory-based formulation [21]. The PDE [Eq. (11)] governing the trajectory ensemble solution  $x^\alpha(X^\mu)$  is second order in *natural* time  $\mathcal{T}$ , and fourth-order in *natural* space  $\mathbf{C}$ , yet treats *inertial*  $t$  and  $x$  on an equal, Lorentz-invariant footing. As a result, the main issues plaguing the traditional wave-based equations of Klein-Gordon and Dirac (when viewed as single-particle theories) are resolved here.

This is especially true for wavepacket dynamics, which serves as the focus of this contribution. Note that even though the traditional wavefunction plays no role in the trajectory formulation, one can nevertheless extract a wavepacket description from the latter—in terms of the inertial probability density quantity,  $j^0$ , which in turn can be obtained from the  $x^\alpha(X^\mu)$  solution itself, together with the natural spatial scalar probability density  $f(\mathbf{C})$ . Unlike wave-based relativistic quantum treatments, the wavepacket dynamics observed here for a free particle are always simple, straightforward, and well-behaved. In particular,  $j^0$  is everywhere positive, localized, and interference-free, with an ensemble-averaged position that travels along a linear path through spacetime. Zitterbewegung and other complications—stemming ultimately from interference between positive- and negative-energy wave solutions—never arise here, because there are no negative-energy trajectory solutions.

We have also examined the symmetry properties of the  $(3 + 1)d$  and  $(1 + 1)d$  dynamical equations, and of their numerically computed Gaussian wavepacket solutions—with respect to parameter and dynamical variable rescaling, as well as Lorentz boosts. The invariance with respect to these symmetry operations has been verified both analytically and numerically. In particular, from scale invariance, we learn that narrowing the initial Gaussian width (by increasing  $a$ ) is essentially equivalent to reducing the speed of light  $c$  (keeping both  $m$  and  $\hbar$  fixed). This makes good physical sense; even in the nonrelativistic context, narrower initial coherent wavepackets are known to disperse more rapidly than broader ones—corresponding in the present context to significant-probability trajectories that approach the speed of light more rapidly. In the extreme ultrarelativistic limit  $c \rightarrow 0$ , one accordingly obtains a Dirac delta initial condition, whose corresponding singular solution has been obtained analytically [21], and may be relevant for cosmology. In the opposite scaling limit, one approaches the standard nonrelativistic Gaussian wavepacket solution—except for the  $|\mathbf{C}| \rightarrow \infty$  “fringe” trajectories that carry almost no probability.

In this work, only the stationary  $x^\alpha(X^\mu)$  solutions were obtained explicitly numerically—although the term “stationary” is a bit of a misnomer, since quantum forces lead to accelerating trajectories that give rise to wavepacket spreading over time. To obtain completely general, moving Gaussian wavepacket solutions, Lorentz-boosting is applied to the stationary solutions. In the wave-based approach, Lorentz boosts in and of themselves can introduce undesirable interference effects [24]. This is not the case for the present trajectory-based approach—e.g., the transformed  $j'^0$  is just as well behaved as  $j^0$ , and  $x^\alpha$  and  $j^\alpha$  exhibit perfect Lorentz invariance.

Numerical solution of the Eq. (17) PDE is complicated by the fact that the boundary conditions are not known *a priori*. The simple remedy proposed here, involving a nonuniform  $\mathbf{C}$  grid, enables higher grid densities and accuracies to be obtained for the physically relevant trajectories that bear significant probability. On the other hand, experience with the nonrelativistic case strongly suggests that this approach will not be so effective in the presence of external fields. Thus, more robust strategies will have to be developed, going forward.

The present work and Ref. [21] serve to demonstrate that the trajectory-based formulation is a very promising approach in the fixed-particle-number relativistic quantum context, worthy of further development. One very convenient feature of this approach is that it derives from a trajectory-based Lagrangian. Thus, both the nonrelativistic and classical limits emerge straightforwardly. Moreover, the Euler-Lagrange and Noether procedures can be directly

applied, to obtain the dynamical PDE and conservation laws, respectively. All of these aspects will be examined in future publications. Another, quite obvious generalization will also be considered: just as the present approach constitutes the trajectory-based analog of the Klein-Gordon equation, by incorporating spin into the theory, we hope to derive the trajectory version of the Dirac equation. Finally, one is not restricted to a trajectory-based approach. Recent work [21] suggests that a mathematically equivalent wave equation can also be developed, which may offer certain advantages, although it would necessarily have to be nonlinear.

## Acknowledgments

This work was supported in part by a grant from the Robert A. Welch Foundation (D-1523). The authors also acknowledge useful discussions with Jeremy Schiff.

## References

- [1] von Neumann J 1932 *Mathematical Foundations of Quantum Mechanics* (New Jersey: Princeton University Press)
- [2] Cohen-Tannoudji C, Diu B and Laloë F 1977 *Quantum Mechanics* (New York: Wiley)
- [3] Bohm D 1979 *Quantum Theory* (New York: Dover)
- [4] Styer D 2002 *Am. J. Phys.* **70** 288
- [5] Bohm D 1952 *Phys. Rev.* **85** 166–179
- [6] Holland P R 1993 *The Quantum Theory of Motion: An Account of the De Broglie-Bohm Causal Interpretation of Quantum Mechanics* (Cambridge, England: Cambridge University Press)
- [7] Einstein A, Podolsky B and Rosen N 1935 *Phys. Rev.* **47** 777–780
- [8] Ballentine L E 1970 *Rev. Mod. Phys.* **42** 358–381
- [9] Home D and Whittaker M A B 1992 *Phys. Rep.* **210** 223–317
- [10] Everett III H 1957 *Rev. Mod. Phys.* **29** 454
- [11] Wheeler J A and Zurek W H (eds) 1983 *Quantum Theory of Measurement* (Princeton: Princeton University Press)
- [12] Bouda A 2003 *Int. J. Mod. Phys. A* **18** 3347
- [13] Holland P 2005 *Ann. Phys.* **315** 505
- [14] Poirier B 2010 *Chem. Phys.* **370** 4–14
- [15] Holland P 2010 *Quantum Trajectories* ed Chattaraj P (Boca Raton: Taylor and Francis/CRC Press) chap 5, pp 73–85
- [16] Poirier B 2011 *Quantum Trajectories* ed Hughes K H and Parlant G (Daresbury Laboratory: CCP6) p 6
- [17] Schiff J and Poirier B 2012 *J. Chem. Phys.* **136** 031102
- [18] Parlant G, Ou Y C, Park K and Poirier B 2012 *Comput. Theoret. Chem.* **990** 3
- [19] Hall M J W, Deckert D A and Wiseman H M 2014 *Phys. Rev. X* **4** 041013
- [20] Poirier B 2014 *Phys. Rev. X* **4** 040002
- [21] Poirier B 2012 Trajectory-based theory of relativistic quantum particles (*Preprint* arXiv:1208.6260 [quant-ph])
- [22] Ryder L H 1996 *Quantum Field Theory* 2nd ed (Cambridge, England: Cambridge University Press)
- [23] Wachter A 2011 *Relativistic Quantum Mechanics* (Dordrecht: Springer)
- [24] Thaller B 2005 *Advanced Visual Quantum Mechanics* (New York: Springer)
- [25] Park S T 2012 *Phys. Rev. A* **86** 062105
- [26] Schweber S S 1961 *An Introduction to Relativistic Quantum Field Theory* (New York: Harper & Row)
- [27] Gross F 1999 *Relativistic Quantum Mechanics and Field Theory* (New York: Wiley)
- [28] Wyatt R E 2005 *Quantum Dynamics with Trajectories: Introduction to Quantum Hydrodynamics* (New York: Springer)